

Elaboration and characterization of graphene-silver nanoparticle hybrids

(NKFI KH-129587, 2018.10.01 – 2020.12.31)

Principal Investigator: Dr. Zoltán Osváth, senior research fellow

The achievements of the project are summarized in six sections below:

1. Preparation and characterization of graphene-silver nanoparticle hybrids on SiO₂ substrates

Thin (5 nm) silver layers were deposited on SiO₂ substrates. Silver nanoparticles (NPs) were prepared by annealing the deposited thin film at 400 °C in argon atmosphere for 90 minutes. The annealing resulted in the formation of hemispherical nanoparticles with high surface coverage and diameters around 20 nm. Graphene grown on copper foil by chemical vapour deposition was transferred on the top of these NPs using thermal release tape (TRT) and an aqueous solution of CuCl₂ (20%) and HCl (37%) to etch the copper. The resulting graphene-silver hybrid nanostructures were characterized by atomic force microscopy (AFM) and confocal Raman spectroscopy. It is known that a thin layer of Ag₂S forms on the surface of silver upon exposure to ambient conditions. We showed that the local heating induced by the laser beam of the Raman instrument decomposed this thin layer of Ag₂S, and this could be monitored *in-situ* on the measured Raman spectra. On graphene-covered NPs we observed more intense graphene Raman peaks (SERS effect), for example the intensity of graphene 2D peak was 8 times larger (after background removal) compared to the graphene 2D peak measured on SiO₂ substrate (Fig. 1a).

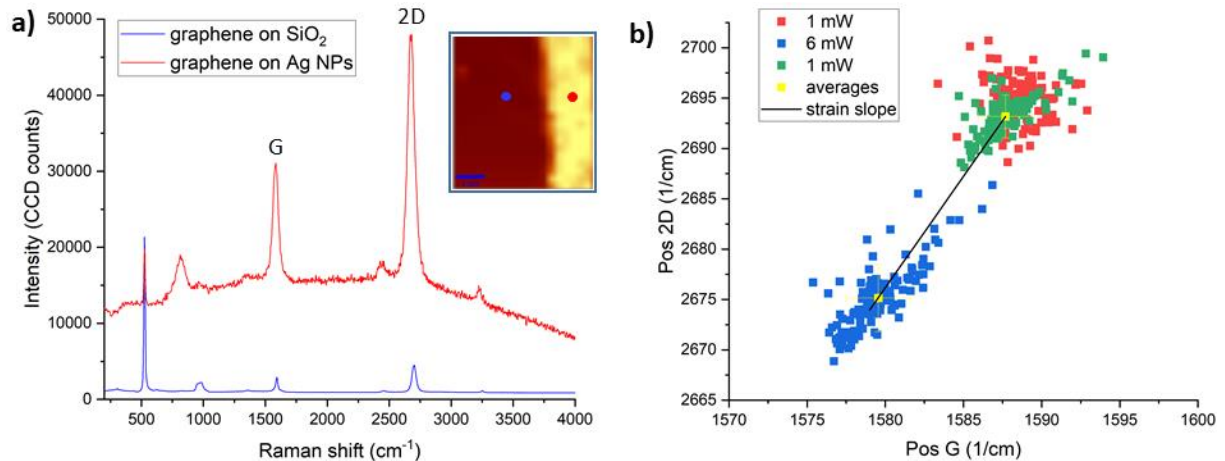


Figure 1. (a) Comparison of graphene Raman spectra measured on SiO₂ substrate (blue line, blue symbol in the inset) and on Ag NPs (red line, red symbol in the inset). The inset shows the Raman map of graphene 2D peak measured on 4x4 μm² area. The area with darker contrast (lower peak intensity) corresponds to graphene on SiO₂ substrate, while the light contrasted area (higher peak intensity) corresponds to graphene on top of Ag NPs. (b) Correlation plot constructed from the position G and 2D peaks measured on graphene supported by Ag NPs. Red and green symbols demarcate low laser intensity (1 mW) measurements performed before (red) and after (green) higher laser intensity (6 mW) measurements marked by blue symbols. The shift of the average values is along the theoretical “strain” line (black).

Raman measurements performed with higher laser intensity (6 mW) induced a dynamic hydrostatic strain (0.23% on average) in the graphene covering the silver NPs, which turned out to be completely reversible upon switching back to measurements using lower (1 mW) laser intensity (Fig. 1b). This effect is similar to what we observed and described earlier on graphene/gold nanoparticle hybrid structures [A. Pálinkás, et al., *Nanoscale* 10 (2018) 13417].

2. Preparation and characterization of graphene-silver nanoparticle hybrids on highly oriented pyrolytic graphite (HOPG) substrates

Thin silver films of 7 nm nominal thickness were evaporated onto HOPG substrates. Immediately after silver deposition and opening of the vacuum chamber, the thin silver films were covered with CVD graphene using TRT, as described in section 1 above. In order to drive the surface diffusion of deposited silver and to form Ag NPs, subsequent annealing of both bare and graphene-covered thin silver films was performed at 400 °C under inert gas (Ar) atmosphere for 90 minutes. We used these annealing parameters that worked earlier for the preparation of gold nanoparticles. The structure and physical properties of the prepared Ag NPs and graphene/Ag NP hybrids were investigated by tapping mode AFM, UV-Vis reflectance spectroscopy, scanning electron microscopy (SEM) and energy-dispersive X-ray spectroscopy (EDX). The graphene-silver nanohybrids were also characterized by scanning tunnelling microscopy (STM) and tunnelling spectroscopy (STS). We compared the differential current-voltage characteristics of HOPG-supported and silver-supported graphene, and we were able to reveal the local *n*-type electrostatic doping of graphene due to charge transfer from silver.

Annealing of the silver thin film resulted in the formation of silver nanoislands with heights around 20 nm and horizontal diameters of 100 nm. We showed that in the case of a graphene overlayer the Ag NPs tend to coalesce and to form larger nanoparticles. We demonstrated that a graphene overlayer preserves the local surface plasmon resonance (LSPR) properties of Ag NPs for at least three months, although the LSPR is gradually redshifted. This is three times longer than the LSPR of bare Ag NPs. We showed by SEM and EDX that graphene can protect Ag NPs from ambient sulphur for more than one year. The SEM image of freshly prepared and partially covered Ag NPs is shown in Fig. 2a. The left part of the image shows bare Ag NPs, while we can observe several graphene-encapsulated groups of Ag NPs on the right part of the image. The shape of NPs is similar in both non-covered and graphene-covered areas. EDX analysis of bare and graphene-encapsulated NPs show characteristic Ag peaks near 3 keV, as shown in Fig. 2b. Additionally, on graphene-covered areas, a Si peak is observed at 1.74 keV (Fig. 2b, black), which is probably due to contamination during graphene transfer (it is missing on areas with bare Ag NPs). The same measurements were performed on samples kept under ambient conditions for 14 months, as shown in Fig. 2c,d. Fig. 5c shows nanoparticles partially covered with graphene. Non-covered nanoparticles are observed in the right part of the image, between the two red lines marking the graphene edges. It is clear that the structure of nanoparticles changed remarkably and they have a less-defined shape after 14 months. In contrast, the graphene-encapsulated NPs observed on the lower left part of Fig. 2c have the same shape as freshly prepared NPs. EDX analysis of aged non-covered nanoparticles (Fig. 2d, red) reveals the presence of sulfur (peak at 2.3 keV), which is the spectroscopic signature of spontaneous sulfurization from air. Importantly, no sulphur is observed by EDX on graphene-encapsulated Ag NPs, even after 14 months (see Fig. 2d). Nevertheless, with the applied transfer process, only 40 – 50% of Ag NPs were coated, and

thus the observed loss of plasmonic properties is primarily attributed to the spontaneous sulfurization of non-covered nanoparticles. A way to improve the long-term stability of LSPR could be to increase significantly the total graphene coverage of Ag NPs. The results were published as an article in the journal *Materials* 13 (2020) 4660.

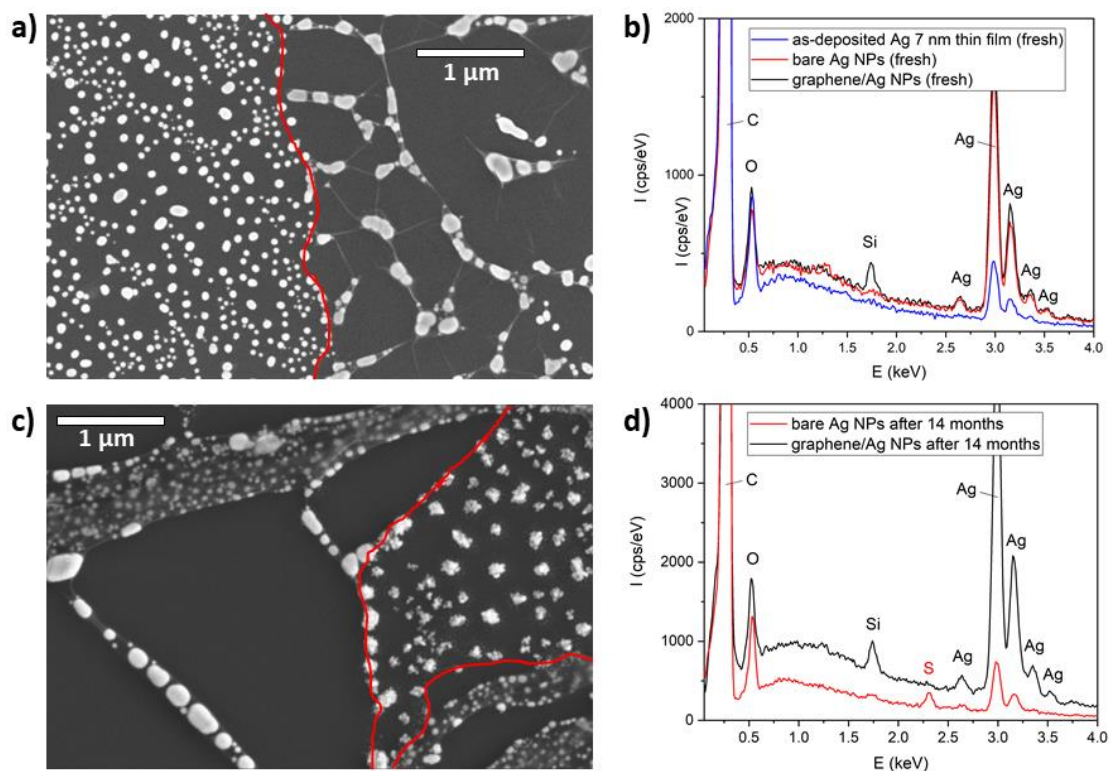


Figure 2. (a) SEM image of freshly prepared Ag NPs partially covered with graphene. The graphene edges are marked with red lines as guides for the eye. (b) EDX spectra measured on freshly prepared 7 nm Ag thin film (blue), bare Ag NPs (red), and graphene–Ag NPs (black). (c) SEM image of Ag NPs partially covered with graphene, 14 months after preparation. Graphene edges are marked with red lines as guides for the eye. (d) EDX spectra measured on bare Ag NPs (red) and graphene–Ag NPs (black), 14 months after preparation.

3. Vapour sensing properties of graphene-covered metallic nanoparticles

Graphene-covered gold nanoparticles were produced and their vapour sensing properties were investigated by measuring the LSPR shift of the gold NPs. We found that smaller, dome-like NPs were more sensitive to ethanol, isopropyl alcohol, and toluene vapours compared to slightly larger, flat NPs. The slope changes observed on the optical response curves of dome-like NPs could be well described by capillary condensation. The fast response and recovery of gold NPs were preserved on the graphene-covered samples as well (see Fig. 3). We demonstrated that the presence of a corrugated graphene overlayer increased the sensitivity to ethanol and isopropyl alcohol, while it decreased it towards toluene exposure (at concentrations $\geq 30\%$). Nevertheless, at low toluene concentrations (10%) where capillary condensation does not yet occur, the graphene covered NPs are more sensitive to toluene, compared to bare NPs. The detection mechanism based on refractive index change does not fully explain the induced LSPR shifts. The interactions between adsorbate, corrugated graphene, and the nanoparticles have to be considered. The results were published as an article in the journal *Nanoscale Advances* 1 (2019) 2408–2415.

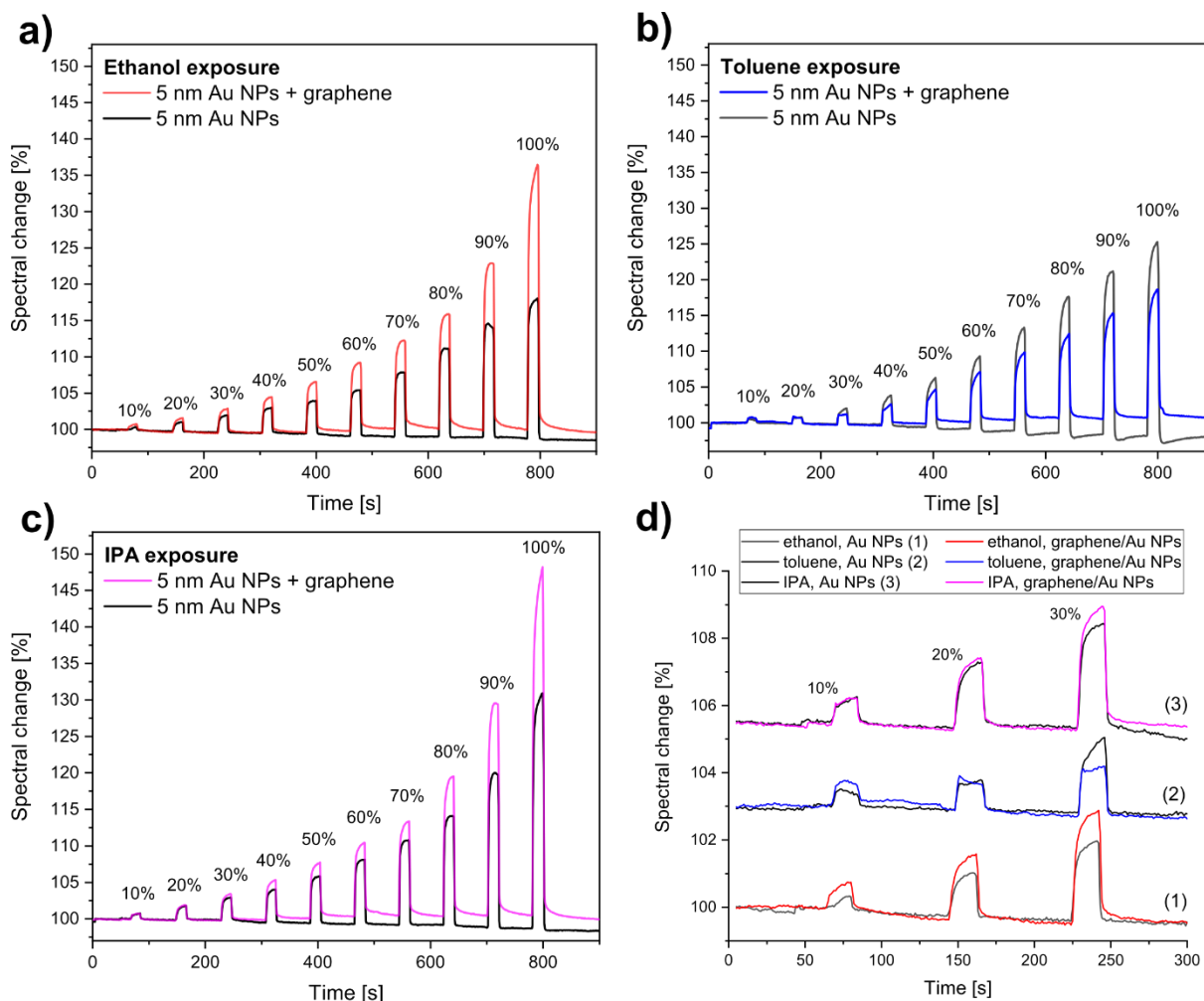


Figure 3. Vapour sensing responses of both bare “5 nm” Au NPs (black lines) and the graphene/“5 nm” Au NPs sample (coloured lines), averaged on 20 nm interval around the maximal spectral change. Exposures to (a) ethanol (b) toluene, and (c) IPA were done for 20 s, followed by purging in synthetic air for 60 s. Vapour concentration steps of 10% were used. Lower concentration ($\leq 30\%$) spectral responses are magnified in (d). The response curves of toluene and IPA exposures were shifted vertically for clarity.

Based on the above findings, similar research was performed with graphene-covered silver nanoparticles as well. Bare and graphene-covered Ag nanoparticles were prepared using the process described above in section 1. The optical reflectance properties of the samples were measured in the wavelength range of 200 to 1000 nm using an Avantes AvaSpec-HS1024 \times 122TEC fibre optic spectrometer. We used a bifurcated probe for illumination and detection with 200 μm core diameters. The reflectance spectra of the samples were recorded by collecting the specular reflected light under normal incidence illumination with an Avantes AvaLight DH-S-BAL balanced UV-Vis light source. Well-defined local surface plasmon resonances are observed at 390 nm and 398 nm for bare and graphene-covered Ag nanoparticles, respectively. In addition, we prepared a graphene/Ag NPs sample which we treated in O_2 plasma for 5 s. The purpose of plasma treatment was to affect the sensing properties of graphene/Ag NPs by introducing large amounts of point defects into the structure of graphene. We examined the effect of plasma treatment by comparing the optical reflectance spectra measured before and after the treatment. Unexpectedly, the plasma

treatment changed significantly the optical response of graphene-covered Ag NPs: its UV absorbance increased dramatically. The LSPR of the sample could be completely recovered by annealing at 400 °C under inert gas (Ar) atmosphere for 90 minutes. This healing effect is attributed to the decomposition of silver oxide, which probably had formed during the O₂ plasma treatment.

Since the LSPR wavelength is sensitive to the environment of nanoparticles, the samples are suitable for carrying out sensing experiments by exposing them to different organic molecules. The adsorption of molecules induces redshift of the LSPR, which can be monitored in-situ. The optical reflectance of graphene-covered Ag NPs and its optical responses to vapour exposure are shown in Fig. 4. Five different analytes were used independently: acetone, ethanol, 2-propanol (IPA), toluene, and water. The maximal optical responses of the sample during saturated vapour exposure were selected and plot together.

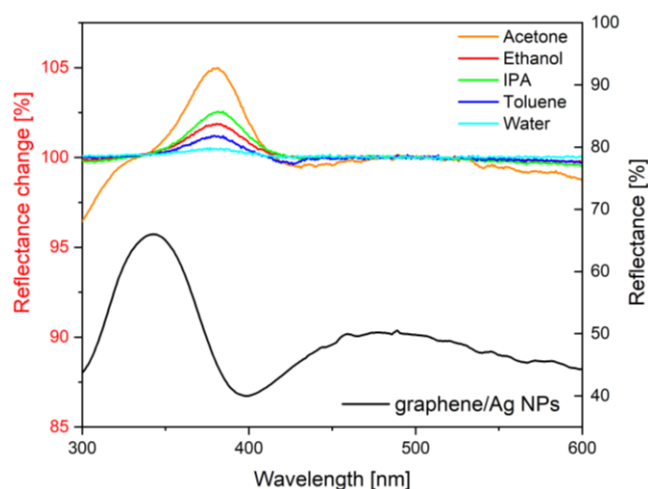


Figure 4. Optical reflectance spectrum (black) and reflectance change signals (coloured) of the graphene-covered Ag NPs during exposure to five different saturated vapours: acetone, ethanol, IPA, toluene, and water. The change is relative to the initial spectrum of the sample in artificial air.

One can observe that the reflectance change of the samples occurs in the LSPR region of the spectrum, between 350 and 450 nm which shows the vapour sensing capability of the graphene-covered Ag NPs. To demonstrate the sensitivity and chemical selectivity of the sample, ten different concentrations were applied during the vapour sensing measurement by diluting the saturated vapours of the five analytes with artificial air (see Fig. 5). Note that the same vapour concentration of two different analytes caused different change in the optical response amplitude. This analyte-specific shift of the LSPR enables the use of these samples for chemically selective vapour sensors. The vapour sensing properties of plasma-treated (and then annealed) graphene/Ag NPs were very similar to the non-treated graphene/Ag NPs. This is tentatively attributed to the healing of graphene point defects through the applied annealing. Nevertheless, the introduction of point defects into the graphene overlayer structure could influence the chemical selectivity in vapour sensing experiments. Mild plasma treatment in argon gas is a possible way to proceed, since the oxidation of Ag NPs in an inert atmosphere is not expected, and thus the annealing step could be skipped.

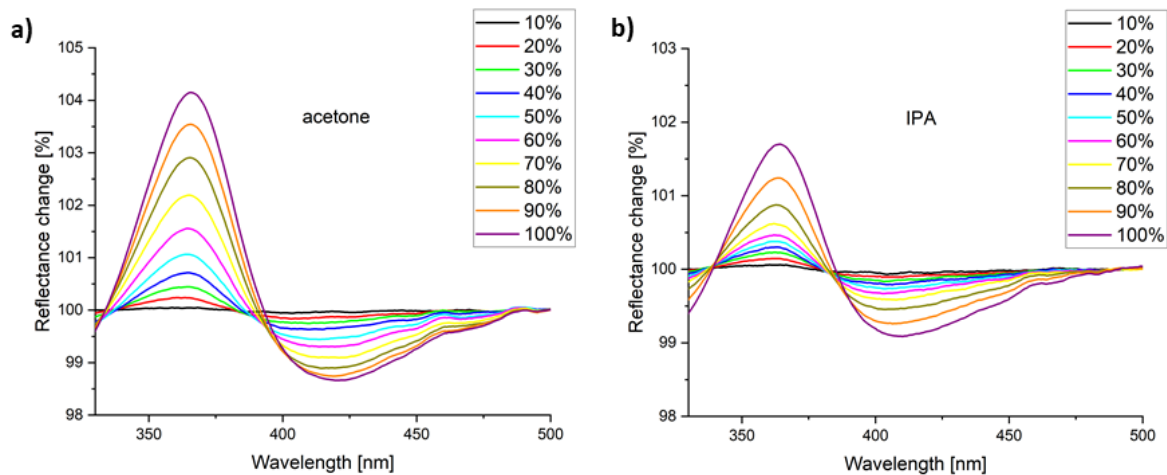


Figure 5. Concentration-dependent vapour sensing measurements carried out using 10% concentration steps from artificial air (0%) to saturated vapours (100%). The optical response of graphene-covered Ag NPs during (a) acetone and (b) IPA exposure (the reference is the initial reflectance in artificial air).

4. Strain effects revealed by anomalous moiré superstructures

When metallic nanoparticles are produced on HOPG substrate and graphene is transferred on them, large areas of graphene-covered HOPG are also prepared on regions with low nanoparticle density. Moiré patterns often form on graphene/HOPG systems and their periodicity depend on the rotational misorientation, as well as on the local bond length differences between graphene and HOPG. The study of moiré patterns is relevant also from the point of view of metallic substrates, since moiré superlattices and anomalous effects can occur on graphene/Ag(111) or graphene/Au(111) systems as well [A. Pálinkás, et al., Carbon 107 (2016) 792].

We studied a small-twist-angle graphene on HOPG by STM/STS. We observed distorted moiré patterns with spatially dependent period. The nanoscale changes in the moiré period observed by STM reflected a locally strained graphene with anisotropic variation of the lattice parameter. We developed a combined graphical-numerical method in order to evaluate the deformations that resulted in these distorted moiré patterns. As a result of our approach, the spatial dependence of the anisotropic deformations was revealed in unprecedented detail: not only the anisotropic moiré pattern could be reproduced, but also the local values of lattice parameters and misorientation angles could be accurately calculated. The sensitivity of the moiré pattern on the variation of graphene parameters was also demonstrated. Additionally, a local density of states (DOS) peak at the Dirac point was observed by room temperature STS measurements, localized at the protruding sites of the moiré pattern, which resulted in a significant increase of the apparent moiré corrugation. These findings were supported by classical molecular dynamics (CMD) simulations, which also revealed direction-dependent bond alternation patterns around the stackings, induced by shear strain. Density functional theory (DFT) calculations confirmed that the measured local DOS peak can be attributed to AAB-stacked trilayer regions in small-twist-angle graphene/HOPG systems. These findings may have implications in the nanoscale strain engineering of the atomic and electronic properties of graphene-based van der Waals heterostructures. The results were published as an article in the journal *Physical Review B* 100 (2019) 125404.

5. Tuning the nanoscale rippling of graphene with PEGylated gold nanoparticles and ion irradiation

Monolayers of Au nanoparticles with diameter of 18 nm, coated with polyethylene glycol (mPEG-SH) were prepared by interfacial assembly. High surface coverage of the NPs was obtained on Si(111) substrates by compressing the trapped monolayer in a Langmuir film balance. Graphene was transferred onto the nanoparticle monolayer. The resulting hybrid material was characterized by Raman spectroscopy, AFM, STM, and STS. We found that the Raman peaks of graphene were not enhanced on the surface-modified nanoparticle monolayer (absence of surface enhanced Raman scattering). This effect was attributed to the mPEG molecules, which increase the distance between graphene and the NPs.

AFM and STM measurements showed that the nanoparticle monolayer formed a quasi-continuous regular (hexagonal) pattern, with period of 20 nm, which is comparable to the periods observed in the moiré superstructures of small-twist-angle graphene bilayers. If such structural periodicity is induced in graphene, the local density of states can significantly change. The quasi-continuity of the nanoparticle monolayer means that there were voids in the layer, corresponding typically to 10 – 50 missing nanoparticles. There, suspended and curved graphene was observed, as it bridged the nanoparticle voids. The ratio between the depth and the diameter of these bowl-like graphene areas was between 5 and 10%. Previously, we used annealing at 400 °C to improve the adhesion of graphene to nanoparticles, and thus to increase its nanoscale rippling. In this case, however, annealing at this temperature induces the transformation of the NPs into larger ones, and thus the regular pattern of the as-prepared nanoparticle monolayer is lost. In order to tune the nanoscale rippling of graphene to match the periodicity of nanoparticles, we introduced point defects in the graphene structure by irradiation with 1 keV Ar⁺ ions using a fluence of the order 10¹² ions/cm². We took advantage of recent findings reported in the literature [e.g. Phys. Rev. B 89 (2014) 201406(R)], which showed that point defects not only modify the local density of states but also induce local deformations in the lattice near the defect. We presumed that sufficiently high density of point defects can tune the nanoscale corrugation of the whole graphene sheet. STM investigations of the graphene/m-PEG/Au NPs hybrid structure performed before and after irradiation revealed that indeed, the rippling of graphene was changed by irradiation and it approximated the periodicity of the underlying nanoparticle monolayer (see Fig. 6).

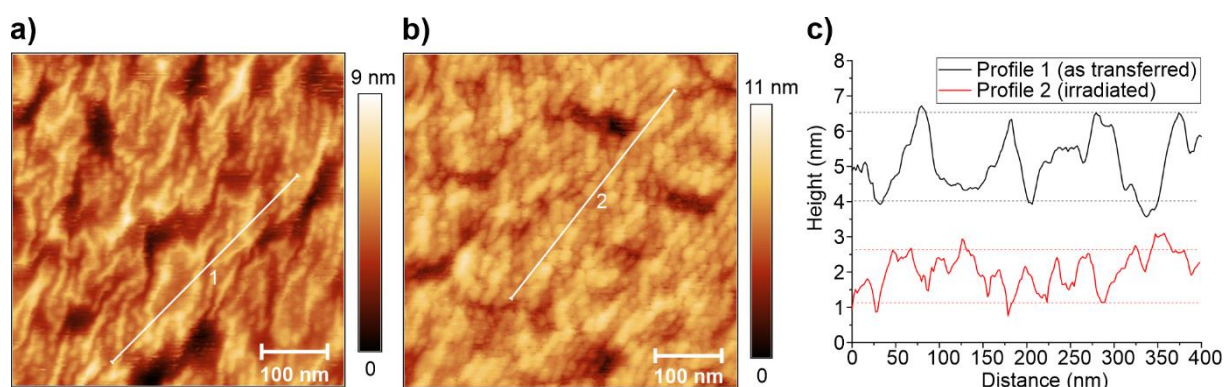


Figure 6. (a) STM image of graphene as transferred onto the gold nanoparticle monolayer. (b) STM image of the nanoparticle monolayer-supported graphene after ion irradiation. (c) The height profiles corresponding to line sections “1” in a) (black line) and “2” in b) (red line). Dashed lines are guide for the eye and denote typical rippling amplitudes: ~2.5 nm in profile “1” and ~1.5 nm in profile “2”.

Furthermore, we observed the signatures of individual point defects by atomic resolution STM (Fig. 7a-b) and also showed by STS the modified local density of states near defect sites (Fig. 7c). A manuscript reporting these results is under preparation.

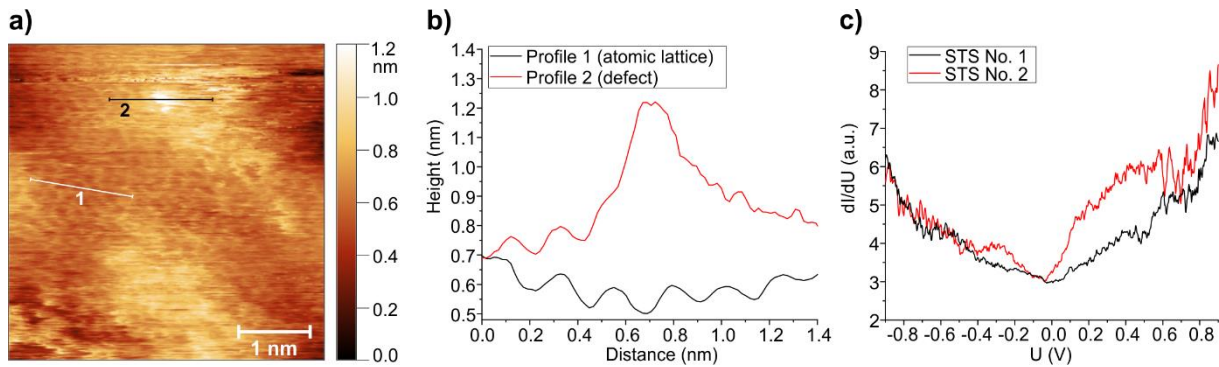


Figure 7. (a) High resolution STM image of the irradiated graphene shown in Fig. 6b. The height profiles corresponding to the line sections 1 (white) and 2 (black) are shown in (b). (c) STS spectra measured on intact (black) and irradiation-damaged (red) graphene areas.

6. Density functional theory (DFT) calculations of metal-supported graphene with atomic defects

We have investigated the effect of the metal substrate on the electronic properties of graphene by using DFT calculations. In order to reveal the interactions between Au(111) and graphene, van der Waals density functional techniques were applied. First, we examined the interlayer distance between Au(111) and graphene and its effect on the electronic properties. For the relaxed interlayer distance, $d=3.45$ Ångström, the V-shape of graphene DOS is still present and only 150 meV p -doping occurs, in good agreement with our previous STS measurements. By decreasing the interlayer distance by 0.5 and 1 Ångström, stronger hybridization of the orbitals takes place, which leads to a metallic character of the graphene (see Fig. 8).

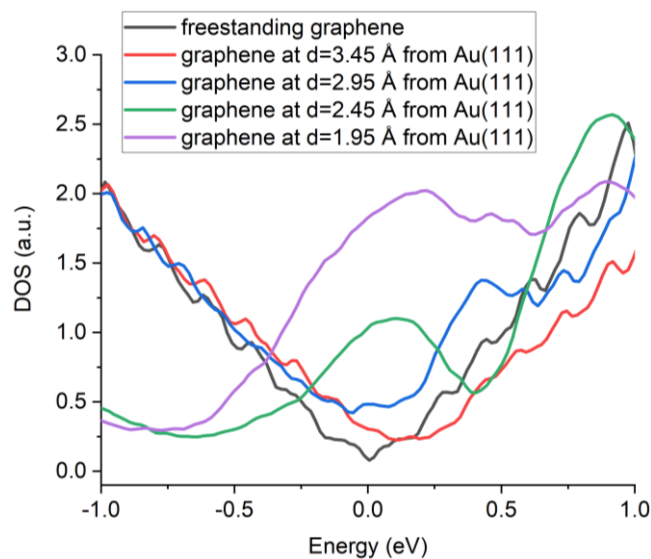


Figure 8. Calculated DOS for freestanding graphene (black) and for gold-supported graphene at different graphene-Au(111) distances: 3.45 Å (red), 2.95 Å (blue), 2.45 Å (green), and 1.95 Å (magenta).

The strongly modified DOS around the Fermi-level from these calculations resemble to the experiments of the annealed graphene/Au samples [A. Pálincás, et al., Carbon 107 (2016) 792]. Therefore, we infer that thermal treatment can decrease the interlayer distance between Au and graphene, resulting modified electronic properties.

As a next step, we have considered an atomic defect, a single carbon atom vacancy in graphene (Fig. 9a). Previous DFT studies [PRL 107, 116803 (2011)] show vanishing magnetic moments of the vacancy due to the non-planar geometry of the relaxed graphene on Pt(111). In contrast, our calculations for Au(111) substrate show negligible out of plane relaxation around the defect, preserving the 2D nature of graphene. In this case the magnetism is associated with the original σ - and π states of the C atoms surrounding the vacancy. The spin-polarized DOS of Au-supported graphene with vacancy is shown in Figure 9b. We observed 10% change of the magnetic moment of the vacancy in the presence of the Au(111) substrate compared to the graphene without substrate.

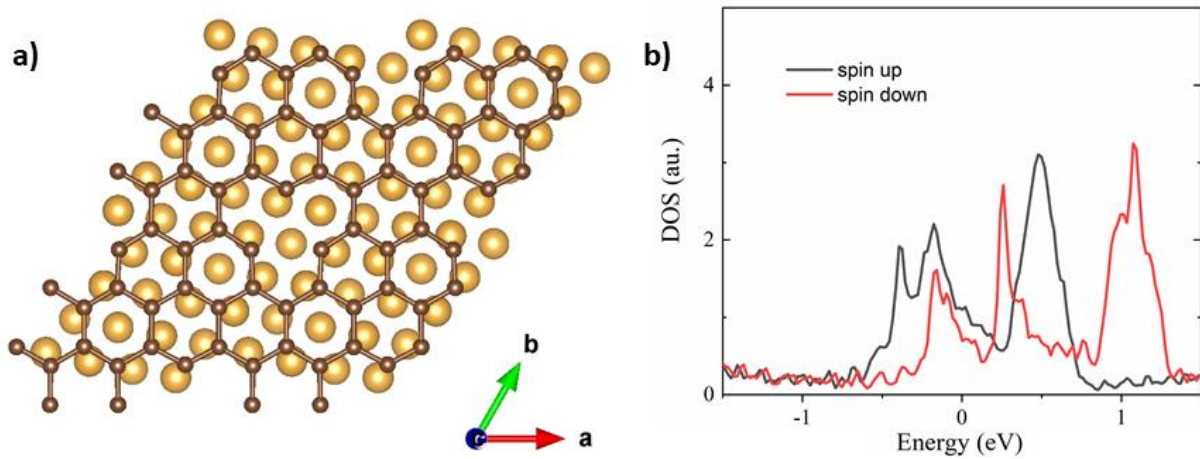


Figure 9. (a) Model of graphene with single vacancy (3x3) on top of Au(111), used in the calculations. (b) Density of states for spin-up (black) and spin-down (red) states of the C atoms surrounding the vacancy.

The slightly changed value of the momentum is originated from the Fermi-level shift caused by the Au(111) substrate [PRL 101, 026803 (2008)]. Similar small changes of the magnetic moment of graphene vacancy on Cu(111) has been reported previously [J. Appl. Phys. 113, 213709 (2013)], where the graphene geometry remained planar after the relaxation. The differences of the relaxation of graphene with vacancy on Pt, Au and Cu substrates could be explained by the different interlayer interactions. In the case of Au(111) and Cu(111) the binding energies are smaller compared to Pt(111), which can preserve the planar structure of graphene and the magnetic moment of the vacancy.